Response of convection to forcing that creates a cold pool

Masaki Satoh[1,2], Shunnosuke Nakai[1], Shuhei Matsugishi[1]

[1] *Atmosphere and Ocean Research Institute, The University of Tokyo, Kashiwa, Japan*

[2] *Typhoon Science and Technology Research Center, Yokohama National University, Yokohama, Japan*

Corresponding author: Masaki Satoh, Atmosphere and Ocean Research Institute, The University of Tokyo, 5-1-5 Kashiwanoha, Kashiwa, 277-8564, Japan. E-mail: satoh@aori.u-tokyo.ac.jp

Submitted to SOLA, September, 24, 2024

Abstract

The cold pool dynamics generated by the evaporation of raindrops in the planetary boundary layer leads to the excitation and organization of convection in the atmosphere. In this study, assuming non-adiabatic cooling due to the evaporation of raindrops, we use numerical simulations to investigate the convection response when a cooling source is forced into the planetary boundary layer. The numerical model SCALE is used to drive a radiative-convective equilibrium state with a horizontal grid spacing of 1 km in a 96 km × 96 km double-period domain. The forcing provides a constant cooling source of 1 K h^{-1} in the region below a height of 1 km. We show that for a forcing width of 2 km or more, convection is localized at both ends of the region in the x-direction, indicating that the effect of the forcing extends over the entire region. The case of a circular forcing also

showed a wider response compared to the forcing radius. A simple model showed that the heat balance between the strength of the mass flux and the heat supply from the sea surface determines the area of expansion of the cold pool.

Keywords: cold pools, radiative-convective equilibrium, convective aggregation

1. Introduction

Convective cold pools generated by the evaporation of raindrops in deep convection play a key role in the excitation and organization of convection. In nature, the intensity of cold pools is influenced by the rainfall intensity in the areas of deep convection and by environmental variables, including wind fields and moisture distributions (Weisman & Rotunno, 2004). The convection sequence via the suppression and excitation of cold pools is complex and involve a variety of processes.

Recently, a number of observational, numerical, and theoretical studies have been conducted on cold pools and their roles in deep convection (e.g., Schlemmer and Hohenegger (2024) and references therein). The global nature of the cold pools is illustrated by a global kilometer-scale model that explicitly resolves the convective system (Sato et al. 2009). Using even higher-resolution numerical simulations, Khairoutdinov and Randall (2006) conducted large eddy simulations (LES) of the diurnal evolution of deep convection with a mesh size of 100 m and compared the time evolution of cloud condensate and precipitation with and without the effect of cold pools. They found that the total amount of cloud condensates and convection frequency decrease when cold pools are artificially suppressed. Fiévet et al. (2023) used LES with an even finer mesh (less than 100 m) to resolve the gust front structure.

Despite the complexity of various processes involved in convective sequence due to cold pools, a simple formula for the cold pool characteristics is useful to understand the underlying mechanisms. One aspect of a cold pool is its role in the suppression and excitation of subsequent convection. A simple formula for estimating the horizontal scale has been derived by Romps and Jeevanjee (2016). We focus on the role of the surface heat flux, which is known to characterize cold pools (Gentine et al. 2016).

To understand the mechanism of a cold pool in suppressing convection, here we isolate the effect of the cold pool forcing in the total evolution of convective systems. We aim to understand the relationship between the forcing intensity and the area of the convective suppression, both of which vary widely in the evolution of realistic convective systems. Thus, we use an idealized framework for the radiative-convective equilibrium in which an artificial forcing is applied. We investigate the results of the convective suppression using a simple formula based on that of Romps and Jeevanjee (2016), with some modifications.

Another aim of this study is to determine whether human forces can alter convective motion in nature. Studies along this line have been conducted (e.g., Horinouchi and Mitsuyuki, 2023) as part of Typhoonshot project (https://typhoonshot.ynu.ac.jp/). We explore various kinds of human intervention to gauge their potential effects on severe storms, focusing mainly on convective systems, to deepenour understanding of the physical mechanisms involved in the excitation of deep convection. The cold pool dynamics is one of the key mechanisms involved in triggering and suppressing deep convection. As a preliminary study of one such intervention in more realistic cases, we examine the effect of cooling in the planetary boundary layer (PBL) on the suppression of convection. In this regard, the strength of the cold pool forcing should be of a magnitude that can be achievable with the limited resources available by human engagement.

In this study, we isolate the effects of cold pools by artificially fixing their strength. Section 2 describes the methodology, including the experimental design and the forcing. Section 3 shows the numerical results. The evaluation of cold pools and their effects are discussed in Section 4. Finally, in Section 5, the summary and the conclusion, together with future directions of research, are described.

2. Methods

We investigated the effect of cold pooling on convection using a radiative-convective equilibrium (RCE) experiment in a limited domain of the regional model. We used SCALE (Scalable Computing for Advanced Library and Environment), which was developed by RIKEN (Nishizawa et al. 2015; Sato et al. 2015). We performed simulations in the double periodic square domain over an *xy*-field of 96 km × 96 km with the top of the domain at an altitude of 33 km. The horizontal grid interval is 1 km, and the number of vertical layers is 74, with a variable vertical level difference of 50-500 m. The lowest level is located at altitude z = 37 m. The Coriolis parameter is set to f = 0, and no diurnal cycle of the solar condition is assumed. The surface temperature is fixed at 300 K. We integrated the simulation for 10 days.

To create a stationary cold pool, we applied a fixed value of cooling in PBL. The cooling intensity is fixed at Q = 1 K h$^{-1,}$ and the top of the forcing is set at an altitude of H = 1 km. This type of direct cooling mimics evaporative cooling by raindrops. As a human intervention, we imagined an engineered method (such as a fountain) that would pump seawater from the sea surface and spray it to a certain height, thereby promoting its evaporation of seawater. Quantitative evaluation using this method is discussed in Section 4.

We tested two types of shape forthe forcing. First, we set up a rectangular region of constant width L km in the x-direction and spanning the entire 96 km in the y-direction (type-I forcing). The lateral width is L = 1, 2, 4, 6 km. These experiments are referred to as L1, L2, L4, and L6, respectively.

For the second type of forcing (type-II forcing), we applied the cooling to a cylindrical domain. The radius of the cooling domain is R = 1, 2, 3, 4, 5, and 6 km, and the forcing center is at $x = y = 48$ km of the square domain. These experiments are referred to as R1, R2, R3, R4, R5, and R6, respectively.

3. Results

For the control experiment without the forcing (CTL), convection is randomly distributed in the simulation domain. When the type-I force is applied at a sufficiently large intensity to the center of the x-direction of the domain, convection is suppressed near the forcing region and generated mainly near the lateral boundary of the domain, which is farthest from the forcing in the periodic boundary condition. Figure 1 shows a snapshot of the outgoing longwave radiation (OLR) of the CTL experiment and the experiment with L = 6 km (L6) (snapshot at t = 10 days). Animations of OLR for CTL and L6 are shown in Figures S1a and S1b, respectively. Figure 2 shows the horizontal distribution of temperature on the the lowest level at t = 10 days (at an altitude of z = 37 m). In the central region near the forcing, the temperature is a few degrees colder than in the outer region. In the *x*-region near the lateral boundaries smaller than about 25 km or more than about 80 km, a clusterof colder temperature also exists. These regions reflect active cold pools that are associated with convection generated near the lateral boundaries of the domain. Convection is suppressed in the inner region of the domain between 25 and 80 km.

Figure 3a shows the distribution of precipitation in the *x*-direction averaged against the *y*-direction and time for the last 90 hours of the 10-day simulation. In CTL, precipitation is present at every location, although it is not yet uniformly distributed because the 90-hour average is too short to be statistically equilibrated. For all forcing experiments L1, L2, L4, and L6, the suppressed precipitation region dominates in the 30–70 km domain. The suppressed region is smaller for the narrowest experiment L1, while the precipitation distribution is almost similar for the rest of the experiments. This result indicates that the suppression of precipitation in L2 is strong enough to push convection to the domain boundary.

Figure 3b is the same as Figure 3a but shows the convective available potential energy (CAPE); CAPE is calculated for an air parcel rising from an alititude of 500 m. CTL shows an almost uniform value for CAPE irrespective of its location. In the forcing experiments, the value of CAPE approaches zero near the center of the domain where the forcing is applied. Toward the convective region at larger or smaller values of *x*, CAPE becomes larger. L2, L4, and L6 have an almost identical and converging distribution. The distribution in L1 is intermediate between those in CTL and L2–L6, with a relatively higher value of CAPE in the convective region. Convection is suppressed in the area where CAPE is smaller than the boundary domain value.

To illustrate the circulation, Figure shows lateral wind speed *U* in the lateral (*x*) and vertical cross-sections in the lower troposphere for L1. Because the height of the cooling is between the surface and the height H = 1 km, the forcing-induced overturning circulation is confined almost to the layer below H. U is divergent near the surface and convergent above the convergence layer. This result suggests that raindrop evaporative cooling in the PBL may induce a shallow overturning circulation in reality.

Figures 5 and 6 show the response to type-II forcing, where the cooling is applied to a cylindrical domain. Figure 5 shows the horizontal distribution of the surface temperature for R6. Near the forcing center at $x = y = 48$ km, a temperature drop of a few degrees is seen in the circle, whose radius is about 10 km. Within a circle of a radius of ~30 km, temperatures are almost uniform, indicating suppressed convection. By contrast, the outer part of this circle shows noisy patterns associated with cold pools of sporadic convection. Figure 6 shows the precipitation distribution for R1, R2, R3, R4, R5, and R6 averaged over the last 90 hours of the 10-day simulation. All the forcing experiments show a convection-suppressed circular region near the center of the domain. The radius of the suppressed region is about 5 km for R1 and about 15, 25, 30, 30, 35, and 40 km for R2, R3, R4, R5, and R6, respectively. That is, the suppressed region is about 5–10 times the radius of the cooling.

4. Estimation of the affected domain

The above results show that the region of suppressed convection is wider than the radius of the forcing. Forcing with constant cooling suppresses convection in an area approximately 5–10 times the radius of the forcing. Cold pools induced by forcing are effective in suppressing convection.

We introduced the forcing intensity of the cooling Q. A typical value of precipitation of convection is about $P_r = 1$ kg m^{-2} h^{-1} for CTL (Fig. 6). If a similar mass of raindrops is evaporated in the PBL whose height is $H = 1$ km, the corresponding cooling rate is

$$Q = \frac{L_f P_r}{\rho H C_p} \sim 2.5 \text{ [K h}^{-1}\text{]},$$

where $\rho \sim 1$ kg m^{-3} is the air density, $C_p \sim 1000$ J kg^{-1} K^{-1} is the specific heat of air at constant pressure and $L_h \sim 2.5 \times 10^6$ J kg^{-1} is latent heat. In the present numerical simulations shown in Section 3, we used the cooling magnitude $Q = 1$ K h^{-1}. This cooling is within the range of realistic values of evaporation cooling of raindrops.

Next, we investigated artificial forcing given by human intervention. We imagine a large fountain that pumps seawater from the sea surface to a height of H and sprays it to the volume V. The distance that a powerful fountain could spray water is assumed to be around 1 km in both height H and horizontal direction L: $V = H L^2 = 1$ km^3. The mass of seawater M required to cool the air in a volume of V by $Q = 1$ K h^{-1} is

$$M = \frac{\rho V C_p Q}{L_h} \approx 400 \text{ [t h}^{-1}\text{]}.$$

This water mass corresponds to the total rainfall in the area L^2 with the precipitation rate $P_r = 0.25$ mm h^{-1}. This value is relatively weak and does not produce a large water vapor supply compared to the existing evaporation associated with convective rainfall.

The power P required to lift the seawater M from the surface to H is

$$P = \frac{MgH}{3600[\text{s}]} \approx 1.1 \text{ [MW]},$$

where $g \sim 10$ m s^{-2} is the acceleration due to gravity. This power would be achievable by renewable energy, such as wind turbines. If we increase the size of the forcing volume V, we would need a number of fountains that is proportional to V.

We estimate the cold pool intensity and the horizontal scale of the suppressed convection. We use the energy budget near the surface in the x-direction with a stationary assumption. A similar and more comprehensive estimation was derived by Romps and Jeevanjee (2016). Here, we focus on a key process that gives a rough estimation of the cold pool and the horizontal scale of the suppression region for the stationary forcing. We assume that the cold pool forcing is $-L < x < 0$, and the surface temperature change is given according to the equation described below (2) in the region $x > 0$.

The temperature decrease at the bottom of the forcing is estimated as $\Delta T_B = QH/W$, where W is the magnitude of the vertical velocity. If we roughly estimate W from the buoyancy $W = (gH\,\Delta T_B/T)^{1/2}$, where g is the acceleration due to gravity, we have

$$\Delta T_B = \left(\frac{Q^2HT}{g}\right)^{\frac{1}{3}}, W = \left(\frac{QH^2g}{T}\right)^{\frac{1}{3}}.$$

This estimate gives $W = 2.1$ m s^{-1} and $\Delta T_B = 0.13$ K for $Q = 1$ K h^{-1}, $H = 1$ km, $T = 300$ K, and $g = 9.8$ m s^{-2}. This derivation of W is based on free fall without any frictional loss or effects of disturbances. In our numerical results, we actually found $W = 0.3$ m s^{-1} so the estimated temperature decrease was $\Delta T_B = 0.9$ K.

The heat balance in the cold pool at the bottom of the forcing region, whose width is L, is given by

$$M_b C_p (T_B - T_0) = \rho C_H u C_p (T_s - T_0) \times L. \qquad (1)$$

where u is the surface wind in the x-direction, C_H is the exchange coefficient of heat, and T_s is the surface temperature (assumed to be uniform). M_b is the mass flux due to the subsidence by the cooling in the PBL and is equal to the lateral mass flux at the lateral boundary of the forcing region $x = 0$: $M_b = \rho h u$, where h is the depth of the cold pool. We assume the wind speed u near the surface on the right-hand side (1) is approximately equal to the lateral wind speed through the depth in the cold pool at $x = 0$. Next, we define

$\Delta T_B = T_s - T_B$, $\Delta T_0 = T_s - T_0$, then

$$\Delta T_0 = \frac{1}{1 + C_H \frac{L}{h}} \Delta T_B.$$

If we use a typical value $C_H = 0.001$ and assume from Figure 4 that L = 1 km and h = 100 m, the temperature difference is $\Delta T_0 = 0.99\, \Delta T_B$. That is, the sensible heat supply from the surface does not significantly affect the temperature in the cold pool within the forcing region.

For $x >$ 0, the heat budget near the surface with a depth of the cold pool h is written as

$$\frac{\partial}{\partial t} \rho h C_p T + \frac{\partial}{\partial x} \rho u h C_p T = \rho C_H u C_p (T_s - T). \qquad (2)$$

Here, we can assume $T = T_0$ at $x = 0$. We denote $\Delta T = T_s - T$ and $M_b = \rho h u$, and assume time independence. The above equation becomes

$$\frac{\partial}{\partial x} M_b \Delta T = -\frac{C_H}{h} M_b \Delta T.$$

The solution is given by

$$\Delta T = \Delta T_0 \exp\left(-\frac{C_H}{h} x\right).$$

Then, the scale of the affected domain is given by

$$A = \frac{h}{C_H} \sim \frac{100\ [m]}{0.001} = 100\ \mathrm{km}.$$

This estimate implies that the horizontal scale of the effective suppression area due to a cold pool by steady-state forcing is about 100 km. In reality, where a cold pool is induced by rainfall from deep convection, the assumption of stationary forcing does not hold. However, if we consider artificial stationary forcing, excitation of deep convection is suppressed in a sufficiently large area with a width of 100 km. This estimation is consistent with the above results of the numerical experiments with type-I forcing. The observed size is in a similar range to this estimation for a specific type of convection over the ocean (Terai and Wood 2013; Zuidema et al. 2017), even though the cold pool is not stationary. In reality, however, the observed horizontal scale is variable because it is sensitive to the type of convection and the environmental conditions (Kirch et al. 2024).

5. Conclusions

We consider the characteristic scale of the cold pool due to cooling in the planetary boundary layer (PBL) by using idealized numerical experiments of radiative-convective equilibrium. This study was also motivated by a hypothetical research question regarding the possibility of deep convection being suppressed by artificial forcing. To this end, we used a stationary forcing in numerical simulations, particularly with cooling in PBL whose depth is about 1 km. The horizontal size of the forcing was assumed to be O(km) and the dependency of the horizontal size is investigated.

We conducted radiative-convective equilibrium experiments in a square domain with 96 km × 96 km. We first assumed an elongated region of the cooling with a width of L km in the x-direction and spanning the entire area in the y-direction. In this case, the deep convection was suppressed throughout almost the entire domain except for the lateral boundaries in the x-direction when $L \geq 2$ km. When we assumed a column region for the cooling with a radius of R km, the deep convection was suppressed in an area of radius about 5–10 times R.

Using the surface energy budget with stationary forcing due to a cold pool, we obtained a characteristic size for the horizontal scale given by h/C_H, where h is the depth of the cold pool, and C_H is the exchange coefficient of heat.

Our results demonstrate that a stationary cold pool generated by the evaporation of raindrops can suppress a sufficiently large domain. Suppose a similar mass of water is lifted to the top of PBL at a height of about 1 km. In that case, we might expect suppression of convection in an area wider than the area of the applied forcing. The method presented here is promising and will be considered for applications in numerical simulations of more realistic convection systems such as typhoons.

Supplements

Animation of the horizontal distribution of OLR [W m^{-2}] for (left) CTL and (right) L6 from t = 0 to 10 days.

Acknowledgments

This study was supported by the Moonshot R&D Grant JPMJMS2282-02 from the Japan Science and Technology Agency and by the JSPS Core-to-Core Program (grant number: JPJSCCA20220001). This study was supported by the Moonshot R&D Grant JPMJMS2282-02 from the Japan Science and Technology Agency and by the JSPS Core-to-Core Program (grant number: JPJSCCA20220001). The Typhoonshot project (https://typhoonshot.ynu.ac.jp/) contributes to the project Moonshot Goal 8, "Realization of a society safe from the threat of extreme winds and rains by controlling and modifying the weather by 2050" in Japan.

Funding

This study was supported by the Moonshot R&D Grant JPMJMS2282-02 from the Japan Science and Technology Agency and by the JSPS Core-to-Core Program (grant number: JPJSCCA20220001).

References

Fiévet, R., B. Meyer, and J. O. Haerter, 2023: On the Sensitivity of Convective Cold Pools to Mesh Resolution. *J. Adv. Model. Earth Syst.*, **15**, e2022MS003382, doi:10.1029/2022MS003382.

Gentine, P., A. Garelli, S. B. Park, J. Nie, G. Torri, and Z. Kuang, 2016: Role of surface heat fluxes underneath cold pools. *Geophys. Res. Lett.*, **43**, 874–883, doi:10.1002/2015GL067262.

Horinouchi, T., and T. Mitsuyuki, 2023: Gross Assessment of the Dynamical Impact of Numerous Power-Generating Sailing Ships on the Atmosphere and Evaluation of the Impact on Tropical Cyclones. *Sci. Online Lett. Atmos.*, **19**, 57–62, doi:10.2151/sola.2023-008.

Khairoutdinov, M., and D. Randall, 2006: High-resolution simulation of shallow-to-deep convection transition over land. *J. Atmos. Sci.*, **63**, 3421–3436. doi:10.1175/JAS3810.1.

Kirsch, B., C. Hohenegger, and F. Ament, 2024; Morphology and growth of convective cold pools observed by a dense station network in Germany. *Q. J. R. Meteorol. Soc.,* **150**, 857–876, doi:10.1002/qj.4626.

Nishizawa, S., H. Yashiro, Y. Sato, Y. Miyamoto, H. Tomita, 2015: Influence of grid aspect ratio on planetary boundary layer turbulence in large-eddy simulations. *Geosci. Model. Dev.*, **8**, 3393–3419.

Romps, D. M., and N. Jeevanjee, 2016: On the sizes and lifetimes of cold pools. *Q. J. R. Meteorol. Soc.*, **142**, 1517–1527, doi:10.1002/qj.2754.

Sato, T., H. Miura, M. Satoh, Y. N. Takayabu, Y. Wang, 2009: Diurnal cycle of precipitation over the tropics simulated by a global cloud resolving model. *J. Clim.*, 22, 4809-4826, doi:10.1175/2009JCLI2890.1.

Sato, Y., S. Nishizawa, H. Yashiro, Y. Miyamoto, Y. Kajikawa, H. Tomita, H., 2015: Impacts of cloud microphysics on trade wind cumulus: which cloud microphysics processes contribute to the diversity in a large eddy simulation. *Prog. Earth Planet. Sci.*, **2**, 23.

Schlemmer, L., and C. Hohenegger, 2014: The formation of wider and deeper clouds as a result of cold-pool dynamics. *J. Atmos. Sci.*, **71**, 2842–2858, doi:10.1175/JAS-D-13-0170.1.

Terai, C. R., and R. Wood, 2013; Aircraft observations of cold pools under marine stratocumulus. *Atmos. Chem. Phys.,* **13**, 9899–9914, doi:10.5194/acp-13-9899-2013.

Weisman, M. L., and R. Rotunno, 2004: “A theory for strong long-lived squall lines” revisited. *J. Atmos. Sci.,* **61**, 361–382, doi:10.1175/1520-0469(2004)061<0361:ATFSLS>2.0.CO;2.

Zuidema, P., G. Torri, C. Muller, and A. Chandra, 2017: A Survey of Precipitation-Induced Atmospheric Cold Pools over Oceans and Their Interactions with the Larger-Scale Environment. *Surv. Geophys.*, **38**, 1283–1305, doi:10.1007/s10712-

017-9447-x.

List of Figure Captions

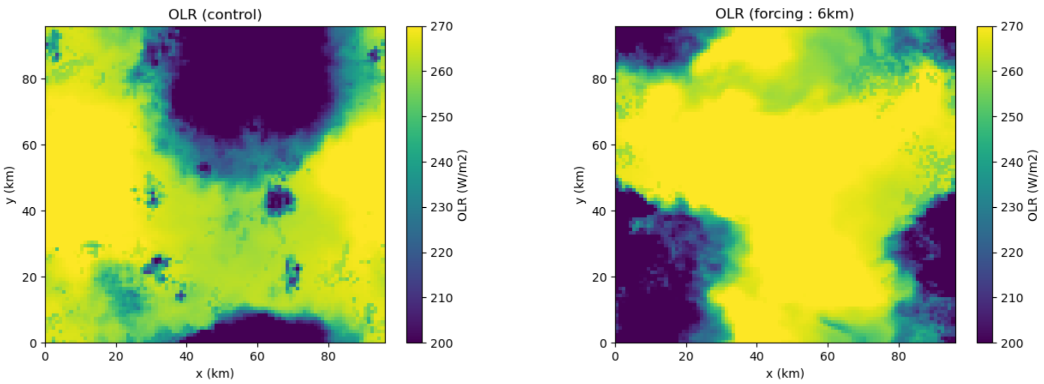

Figure 1. The horizontal distribution of OLR [W m^{-2}] for (left) CTL and (right) L6 at t = 10 days.

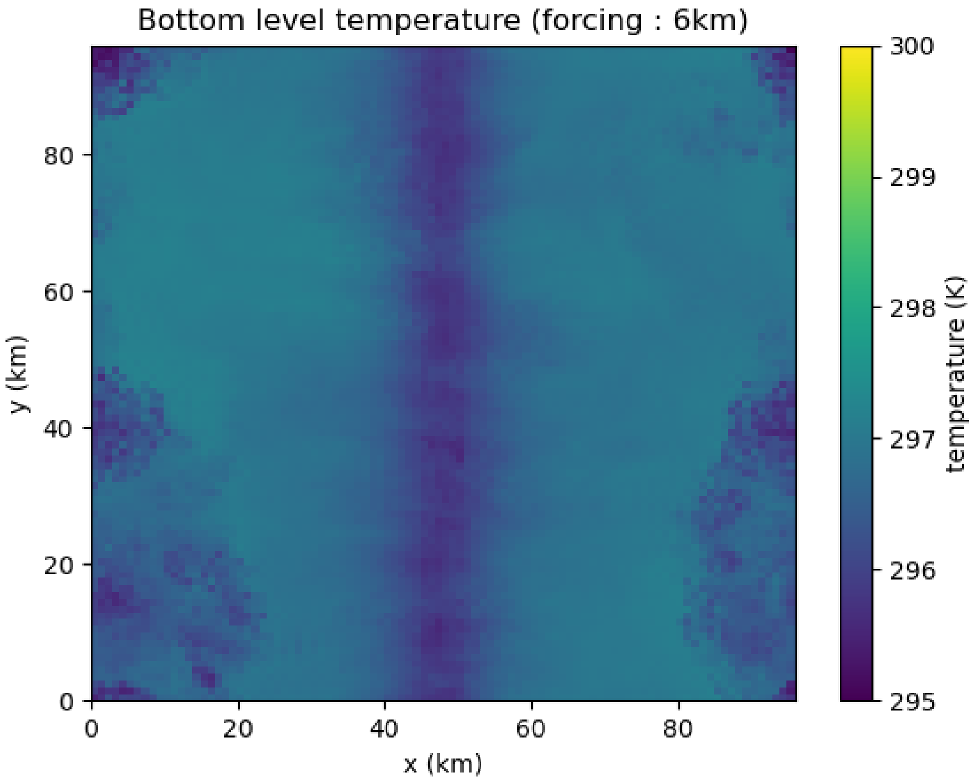

Figure 2. The horizontal distribution of bottom level (z = 37 m) temperature [K] for L6 at t = 10 days.

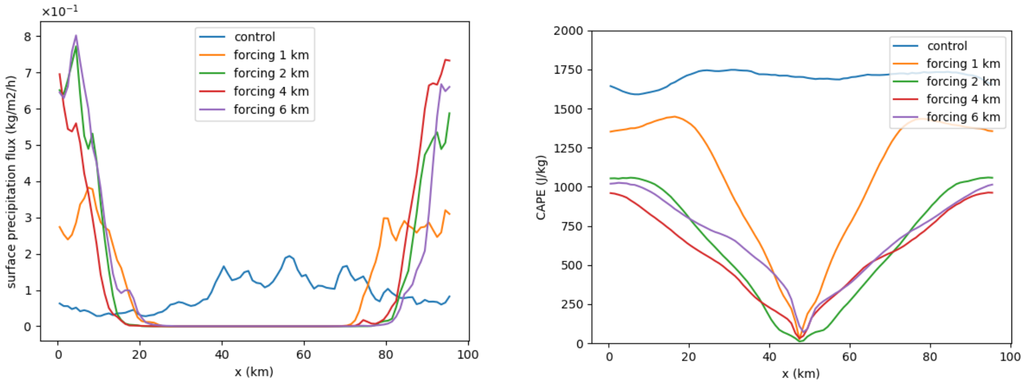

Figure 3. The x-distribution of precipitation [kg m^{-2} h^{-1}] (left) and CAPE [J kg^{-1}] (right) averaged over the y-direction and time for the last 90 hours of the 10-day simulation.

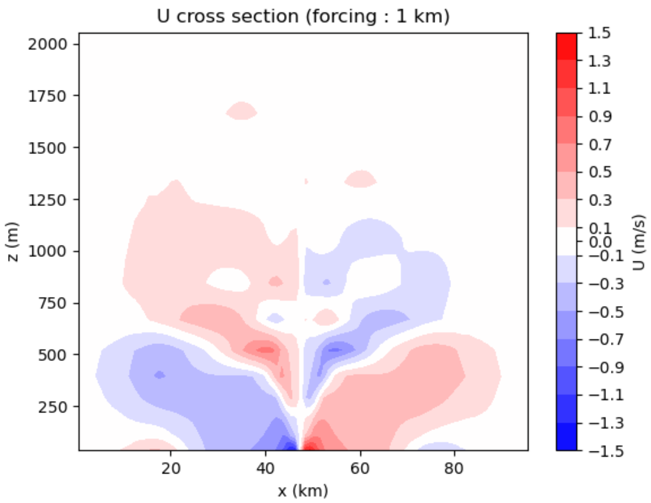

Figure 4. The lateral-vertical cross-section distribution (the *xz*-plane) of the lateral (*x*) velocity [m s^{-1}] averaged over the *y*-direction and time for the last 90 hours of the 10-day simulation.

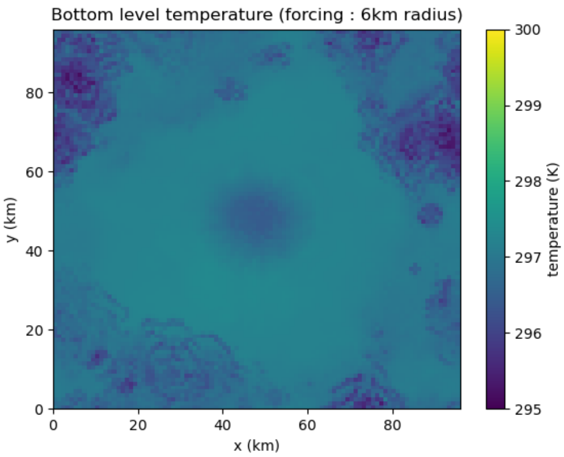

Figure 5. The horizontal distribution of bottom-level (z = 37 m) temperature [K] for R6 at t = 10 days.

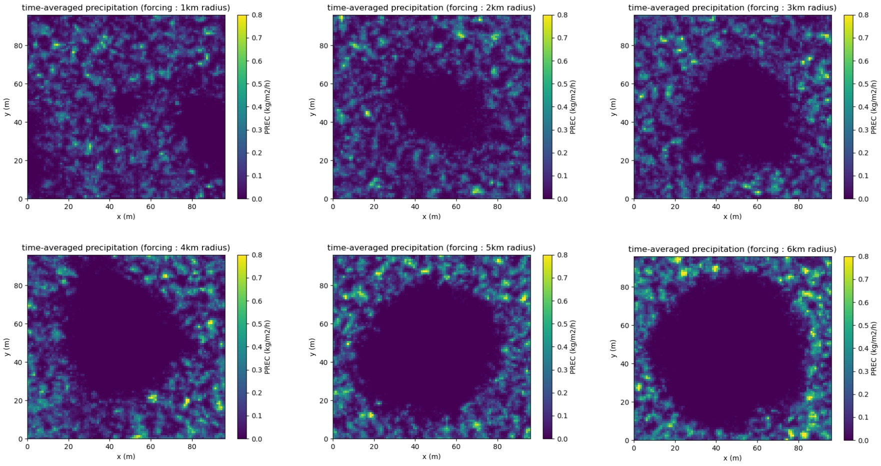

Figure 6. The horizontal distribution of precipitation [kg m^{-2} h^{-1}] for R1, R2, and R3 (top, left to right) and R4, R5, and R6 (bottom, left to right).

.

Figure S1 (please see the supplementary file for animations)

Animation of the horizontal distribution of OLR [W m^{-2}] for (left) CTL and (right) L6 from $t = 0$ to 10 days.